RSC Advances




ROYAL SOCIETY OF CHEMISTRY

www.rsc.org/advances

RSC Advances

Dynamic Article Links ►

Cite this: DOI: 10.1039/c0xx00000x

www.rsc.org/xxxxxx

ARTICLE

# Guanidine-functionalized $Fe_3O_4$ magnetic nanoparticles as basic recyclable catalysts for biodiesel production

**Evelyn C. S. Santos,[a] Thiago C. dos Santos,[a] Renato B. Guimarães,[b] Lina Ishida,[c] Rafael S. Freitas,[c] Célia M. Ronconi*[a]**

***Received (in XXX, XXX) Xth XXXXXXXXX 20XX, Accepted Xth XXXXXXXXX 20XX***
**DOI: 10.1039/b000000x**

Two organic superbases, 1,5,7-triazabicyclo[4,4,0]dec-5-eno (TBD) and 1,1,3,3-tetramethylguanidine (TMG), were anchored onto silica-coated and uncoated iron oxide nanoparticles, resulting in three (MNP-TBD, MNP-TMG and MNP@$SiO_2$-TBD) recoverable basic nanocatalysts. The nanocatalysts were fully characterized by elemental analysis, infrared and Raman spectroscopies, X-ray diffraction, transmission electron microscopy, $N_2$ adsorption/desorption isotherms, thermogravimetric analysis and magnetic measurements. X-ray diffraction indicated the presence of spinel-structured iron oxide, and Raman spectroscopy revealed both magnetite and maghemite phases in the prepared nanocatalysts. The average particles sizes of the nanocatalysts were in the range of 11 to 12 nm, and they exhibited superparamagnetic behaviour at 300 K. Infrared spectroscopy indicated the presence of the superbases (TBD and TMG) on the surface of the silica-coated and uncoated iron oxide nanoparticles. The performance of the nanocatalysts was tested in the methanolysis reaction of soybean oil under different conditions. At the end of each reaction, the nanocatalysts were magnetically recovered from the medium, and the product was analysed and quantified by high-performance liquid chromatography (HPLC). MNP-TBD exhibited the best catalytic performance in the first cycle (96% biodiesel conversion); however, MNP@$SiO_2$-TBD exhibited the best reusability.

## Introduction

Petroleum is a non-renewable source of energy; therefore, the development of technologies to generate energy from renewable feedstock remains a major societal need.[1] Biodiesel is garnering attention as an alternative fuel derived from vegetable oils or animal fats. This fuel is considered to be safer, more biodegradable and to cause less pollution than traditional diesel.[2,3,4] Biodiesel is produced by the transesterification process catalysed by acids, bases or enzymes in the presence of methanol. Industrial production is carried out under homogeneous basic catalysis using hydroxides and alkoxides of alkaline-earth metals to achieve high yields.[5,6] Catalyst recovery, however, is one of the limitations of the process.[7,8] In addition, the remaining catalyst should be removed during water washings; however, to our knowledge, the maximum residual concentration of catalysts in biodiesel is not specified by the American Society for Testing and Materials (ASTM). Excess residual basic or acid catalysts can cause fuel tank corrosion and other engine problems. To overcome this limitation, immobilization of the catalysts onto various solid supports facilitates their recovery. Hydrotalcites,[9,10] modified zeolites[11,12] and metal oxides[13,14] are among the solids investigated to date. Furthermore, catalytic compounds such as guanidines have been supported on mesoporous silica (MCM-41)[15,16,17,18] and subsequently used in transesterification reactions.[19,20,21,22] Previously, we have demonstrated 99% biodiesel conversion using the guanidine 1,5,7-triazabicyclo[4,4,0]dec-5-eno (TBD) anchored onto MCM-41.[20] However, the biodiesel conversion rate decreases drastically to 0.8% after the fifth cycle, likely because of neutralization of basic sites on the guanidine by free fatty acids contained in soybean oil.

In the field of catalysis, magnetic nanoparticles (MNPs) are interesting and versatile materials because of their high surface-area-to-volume ratio, which facilitates surface modification.[23] Thus, MNPs are an alternative support material because of their easy synthesis and functionalization, low cost, and low toxicity.[24] The greatest advantage of MNPs is their easy recovery from the reaction medium under an applied external magnetic field, eliminating steps such as centrifugation, filtration, and extraction.[25,26,27,28] To protect MNPs from external attack and avoid agglomeration, a thin coat of silica can be deposited onto their surface, giving rise to a core-shell structure.[29] Subsequently, this silica shell can be functionalized with a coupling agent such as 3-(chloropropyl)triethoxysilane (CPTES) to enable further surface modifications.

In this work, we successfully anchored two organic superbases, TBD and 1,1,3,3-tetramethylguanidine (TMG), onto silica-coated and uncoated magnetic supports, resulting in three (MNP-TBD, MNP-TMG and MNP@$SiO_2$-TBD) recoverable basic nanocatalysts (Scheme 1). The catalysts were prepared in

three steps: (i) synthesis of $Fe_3O_4$ nanoparticles *via* co-precipitation of Fe(II) and Fe(III) ions from basic solution; (ii) surface modification with chloropropyl groups; and (iii) functionalization with guanidine bases through $S_N2$ nucleophilic substitution of the chloro-functionalized $Fe_3O_4$ nanoparticles. For the preparation of the silica-coated magnetic nanocatalyst, tetraethylorthosilicate (TEOS) was added to the reaction medium containing $Fe_3O_4$ nanoparticles and guanidine functionalization was performed as previously described (Scheme 1). The characterization results for the three materials and the results of an evaluation of their catalytic properties towards biodiesel production are presented. We also discuss the differences in performance among the three materials.

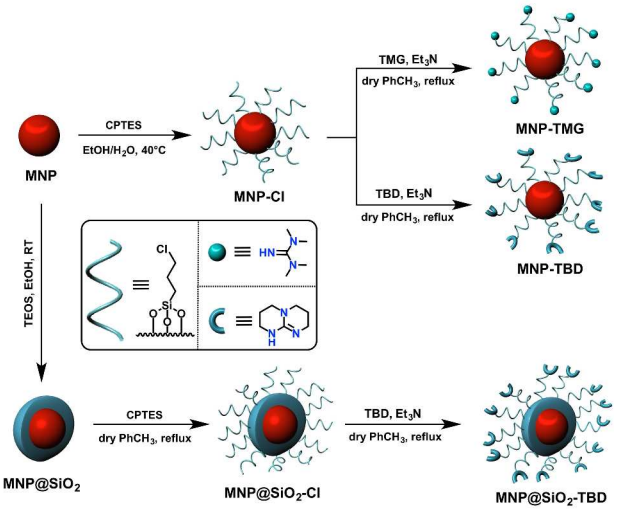


**Scheme 1** Synthesis of magnetic silica-coated and uncoated catalysts (MNP-TBD, MNP-TMG and MNP@$SiO_2$-TBD).

## Results and discussion

### Characterization of the catalysts

On the basis of CNH elemental analysis, the amount of guanidine base present on each magnetic nanocatalyst was 0.20, 0.16 and 0.3 mmol $g^{-1}$ of MNP-TBD, MNP-TMG MNP@$SiO_2$-TBD, respectively.

Fig. 1 shows the FT-IR spectra of the magnetic nanocatalysts and their precursors. The IR spectrum of the $Fe_3O_4$ MNPs showed a large, broad band at 3414 $cm^{-1}$ associated with the stretching vibration of O-H groups on their surface.[30] An intense band due to Fe-O bond vibrations was split into two peaks at 635 and 570 $cm^{-1}$. This band splitting has been associated with the nanometric size of $Fe_3O_4$ MNPs and was observed for all of the prepared catalysts and their precursors.[31] Grafting of 3-(chloropropyl)triethoxysilane onto MNP-Cl was confirmed by the bands at 998 $cm^{-1}$, 1124 $cm^{-1}$ and 2861 to 2938 $cm^{-1}$, which are assigned to the Fe-O-Si,[32] Si-O-Si[33] and C-H stretching vibrations,[34] respectively. The band at 998 $cm^{-1}$ was not observed in the spectrum of the silica-coated material because of the presence of a strong and broad stretching vibration band of the siloxane groups (Si-O) at 1007 $cm^{-1}$. The bands at 1440 $cm^{-1}$ and 1625 $cm^{-1}$ present in the spectra of guanidine-functionalized magnetic nanocatalysts correspond to C-N and C=N stretching vibrations of the guanidines, respectively.[35,36] These latter bands indicate that the guanidine bases were grafted onto silica-coated and uncoated magnetic supports.

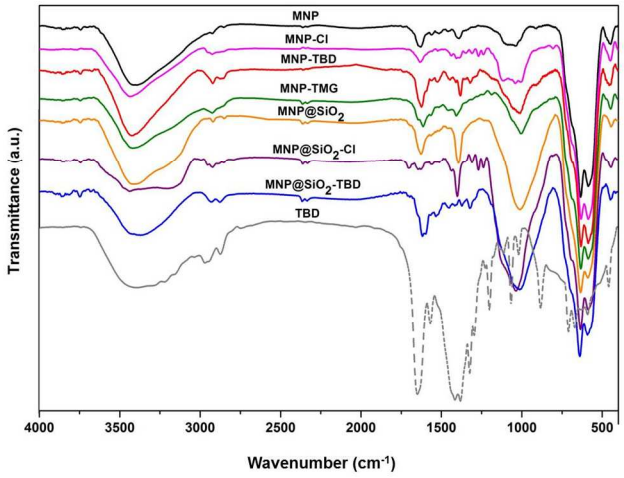


**Fig. 1** FTIR spectra of the magnetic nanocatalysts (MNP-TBD, MNP-TMG and MNP@$SiO_2$-TBD) and their precursors.

X-ray diffraction (XRD) patterns of the MNPs and the nanocatalysts (Fig. 2) indicate the presence of a spinel-structured oxide identified as either as magnetite ($Fe_3O_4$) or maghemite ($\gamma$-$Fe_2O_3$).[37] The XRD pattern of MNP@$SiO_2$-TBD did not show peaks related to the silica, probably because of the thinness of the shell.

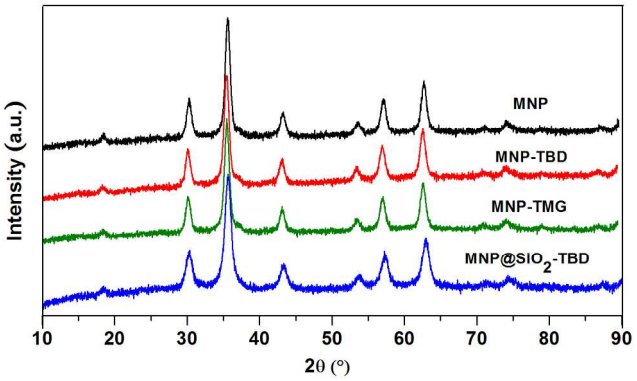


**Fig. 2** XRD patterns of the $Fe_3O_4$ MNPs and the magnetic nanocatalysts.

Raman spectroscopy can be used to distinguish both phases of iron oxides.[38] A confocal Raman microscope was used to collect the spectra of all of the nanocatalysts (Fig. 3 and Fig. S1, see ESI†). Spectra were collected at several regions of each sample. All of the spectra exhibit a main band at approximately 666 $cm^{-1}$ that is assigned to the symmetric stretch of oxygen atoms along Fe–O bonds ($A_{1g}$) of magnetite; the bands at approximately 717 ($A_{1g}$), 500 ($T_{2g}$) and 357 ($E_g$) $cm^{-1}$ are associated with maghemite.[39] Thus, all of the prepared catalysts are composed of both the magnetite and maghemite phases of iron oxide.

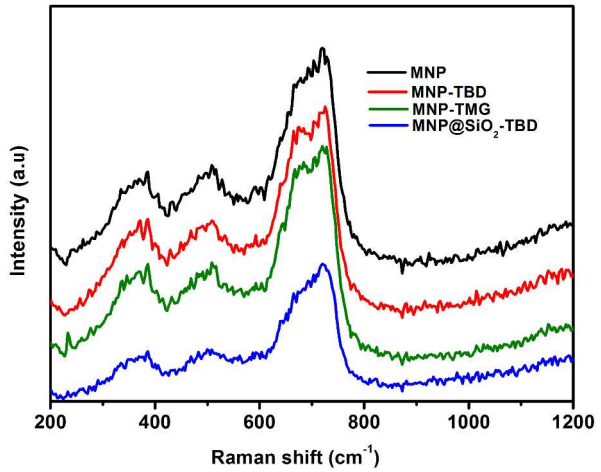


**Fig. 3** Raman spectra of the $Fe_3O_4$ MNPs and the magnetic nanocatalysts.

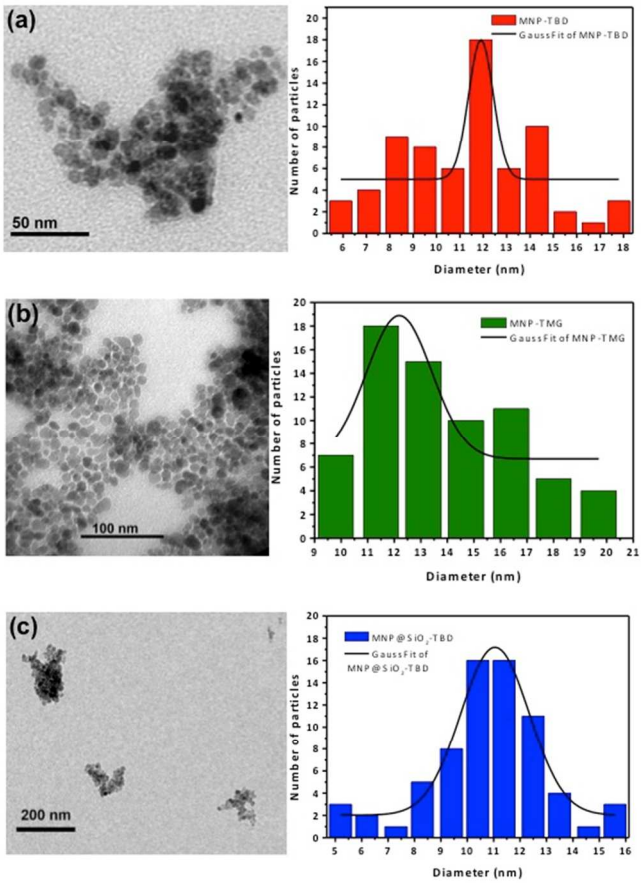


**Fig. 4** TEM images and particle-size distributions (PSDs) of (a) MNP-TBD, (b) MNP-TMG and (c) MNP@$SiO_2$-TBD.

Transmission electron microscopy (TEM) of MMP-TBD, MNP-TMG and MNP@$SiO_2$-TBD show spherical particles (Fig. 4). The particle-size distribution curves (Fig. 4) indicate that the average particle diameters of MNP-TBD, MNP-TMG and MNP@$SiO_2$-TBD are 12, 12.3 and 11 nm, respectively. The average sizes of $Fe_3O_4$ nanoparticles obtained by the co-precipitation method, in which the base is rapidly injected, are typically smaller and more uniform than those obtained by the conventional co-precipitation method.[40] Fast injection of the base ($NH_4OH$) results in a fast nucleation process, yielding small particles. TEM images of MNP@$SiO_2$-TBD show a uniform and continuous silica shell around the surface of $Fe_3O_4$ particles (Fig. S2, see ESI†).

$N_2$ adsorption/desorption isotherms of the nanocatalysts (Fig. S3, see ESI†) are of type IV in the IUPAC classification, which is typical of mesoporous materials. The presumed mesoporosity of the nanocatalysts is probably related to spaces between the nanoparticles arising from their aggregation,[36,41] as evident in the TEM images. The Brunauer-Emmett-Teller (BET) specific surface areas are 62 $m^2\ g^{-1}$, 53 $m^2\ g^{-1}$ and 84 $m^2\ g^{-1}$ for MNP-TBD, MNP-TMG and MNP@$SiO_2$-TBD, respectively. The BET surface area of the MNP@$SiO_2$-TBD catalyst was greater than those of the other catalysts because of the presence of the silica shell.

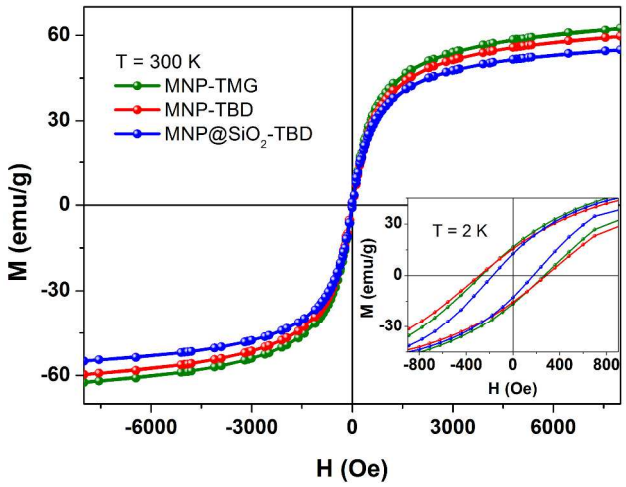


**Fig. 5** Field dependence of the magnetization measured at 300 K and 2 K (inset) for MNP-TBD, MNP-TMG and MNP@$SiO_2$-TBD.

Fig. 5 shows the field dependence of the magnetization for all three nanocatalysts at room temperature. The absence of hysteresis indicates the superparamagnetic nature of the nanocatalysts at T = 300 K. The saturation value of the magnetization at this temperature and at a magnetic field of 70 kOe corresponds to approximately 70 emu/g of nanocatalyst.

Fig. 6 shows the temperature dependence of the zero-field-cooled (ZFC) and field-cooled (FC) magnetization of the three nanocatalysts. The blocking temperature $T_B$ of the magnetic moment is indicated by the maximum in the ZFC curve. The silica-coated nanocatalyst MNP@$SiO_2$-TBD exhibits a lower blocking temperature as well as a lower coercivity at low temperatures (inset of Fig. 5) compared to those of the other nanocatalysts. This result is commonly explained as a consequence of the surface anisotropy reduction due to the silica coating.[42]

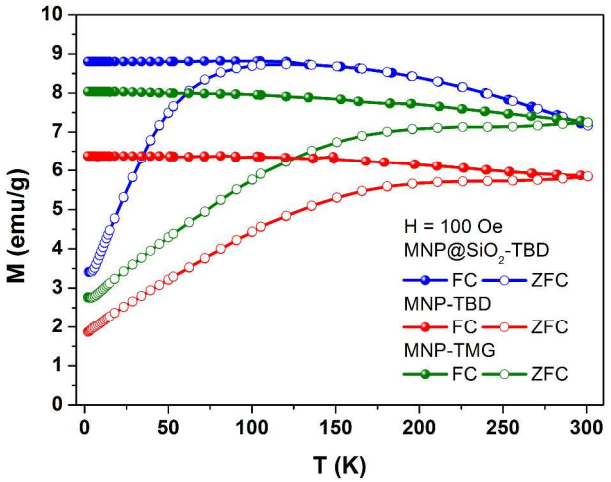


**Fig. 6** Field-cooled (closed symbols) and zero-field-cooled (open symbols) magnetization of the nanocatalysts measured at 100 Oe.

Thermogravimetric analysis (TGA) of all of the prepared nanocatalysts (Fig. S4, see ESI†) was conducted to verify their thermal stabilities and to establish the appropriate temperature for the catalytic reactions. The TGA curves show two main decomposition steps. The initial weight loss of approximately 1% is likely due to the presence physisorbed water or solvent molecules on the surface of the nanocatalysts. The data suggest that the second step, at temperatures ranging from 200 to 600 °C, comprises two consecutive weight losses. Both are related to the decomposition of the organosilane and the guanidine bases grafted onto the MNPs. The weight loss during this step is approximately 8.6, 8.0, and 9.0 wt% for MNP-TBD, MNP-TMG and MNP@$SiO_2$-TBD, respectively. These results corroborate the relative quantities of guanidine estimated by elemental analysis for each nanocatalyst. In addition, the nanocatalysts were demonstrated to be thermally stable at the temperature used for the transesterification reaction (120 °C).

### Catalytic activities of the MNP-TBD, MNP-TMG and MNP@$SiO_2$-TBD catalysts towards biodiesel production

To evaluate the catalytic activities of the guanidine-functionalized $Fe_3O_4$ superparamagnetic nanoparticles and to determine the most appropriate reaction conditions, the transesterification reaction of soybean oil with methanol was investigated (Table 1).

**Table 1** Methanolysis of soybean catalysed by MNP-TBD, MNP-TMG and MNP@$SiO_2$-TBD at 120 °C, using 10% for each catalyst

| Entry | Catalyst | MeOH/oil | Time (h) | Biodiesel yield (%) |
|---|---|---|---|---|
| 1 | None | 30:1 | 24 | 0 |
| 2 | MNP-TBD | 30:1 | 24 | 96 |
| 3 | MNP-TMG | 30:1 | 24 | 11 |
| 4 | MNP-TBD | 30:1 | 12 | 78 |
| 5 | MNP-TBD | 30:1 | 6 | 60 |
| 6 | MNP-TMG | 30:1 | 6 | 9 |
| 7 | MNP@$SiO_2$-TBD | 30:1 | 24 | 80 |

The results in Table 1 show that the MNP-TBD was an efficient nanocatalyst in the transesterification reaction of soybean oil at 120 °C and at a 30:1 methanol-to-oil molar ratio. The biodiesel yield was 60% after 6 h (entry 5) and 96% after 24 h (entry 2). Thus, the biodiesel yield increases with increasing reaction time. Using the MNP@$SiO_2$-TBD nanocatalyst resulted in an 80% biodiesel yield after 24 h (entry 7), which is close to the yield obtained using the MNP-TBD catalyst. MNP-TMG nanocatalyst was the least efficient, yielding only 11% biodiesel at the same reaction time (entry 3). Control experiments showed that, in the absence of the nanocatalysts, no biodiesel conversion was observed under the same reaction conditions (Table 1, entry 1).

Table 2 shows the turnover number (TON), which is expressed as yield per mmol of basic sites, and the turnover frequency (TOF), which is expressed as TON per hour during the experiments. Because the kinetics of the reactions were not investigated, the TON values calculated in this work provide only a trend for the activity of the nanocatalysts.

The MNP-TBD nanocatalyst exhibits the highest TON and TOF, followed by the MNP@$SiO_2$-TBD and the MNP-TMG nanocatalysts. The higher TON and TOF for the MNP-TBD and MNP@$SiO_2$-TBD compared to those for the MNP-TMG are attributed to the intrinsic basicity of the guanidines. TMG and TBD are considered organic superbases because of the resonance stability of their conjugated acids.[43] The $pK_a$ of TBD is 25.9 ($CH_3CN$), whereas that of TMG is 23.3 ($CH_3CN$). The six-membered ring of TBD increases its basicity compared to the acyclic TMG. The transesterification reaction homogeneously catalysed by TMG (10%) under reflux conditions produced a biodiesel yield of 75% biodiesel after 1 h of reaction, whereas TBD yielded 97%. However, heterogenization of TMG drastically decreased its catalytic performance. Both superbases were anchored to the magnetic nanoparticles modified with 3-(chloropropyl)triethoxysilane by the amine nitrogen, leaving the *N* imino atoms available to carry out methanol deprotonation (Fig. S5, see ESI†). Compared to the *N* imino atoms of TBD in a heterogeneous phase, those of TMG are likely much less accessible to the methanol molecules because of steric effects.

**Table 2** Activity, expressed in TON and TOF, and basicity, expressed in terms of the $pK_a$, of the catalysts.

| Catalyst | TON[a] | TOF[b] |
|---|---|---|
| MNP-TBD | 480 | 20 |
| MNP-TMG | 69 | 3 |
| MNP@$SiO_2$-TBD | 267 | 11 |

[a] (% biodiesel per mmol of basic sites).

[b] (TON/h).

### Reusability and recovery of the MNP-TBD and MNP@$SiO_2$-TBD nanocatalysts

The reusability and recovery of MNP-TBD and MNP@$SiO_2$-TBD were investigated. Nanocatalyst recovery after the reactions was very simple and easy, as shown in Fig. 7.

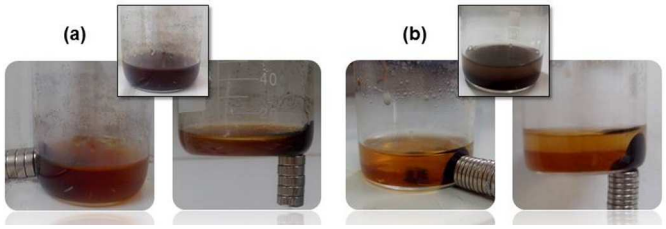


**Fig. 7** Images showing the crude products obtained after the transesterification reaction before and after an external magnetic field was applied: (a) MNP-TBD and (b) MNP@$SiO_2$-TBD.

The reusability of the MNP-TBD and MNP@$SiO_2$-TBD catalysts was evaluated under the conditions described in Table 1 (entry 2 for MNP-TBD and entry 7 for MNP@$SiO_2$-TBD). After each reaction cycle, the nanocatalysts were separated from the reaction mixture using a magnet, recovered, washed with methanol, and then washed with 0.1 mol $L^{-1}$ NaOH aqueous solution and deionized water until the nanoparticle suspension reached a pH of 7. The nanocatalysts were air-dried before being reused in the next cycle. Washings with aqueous NaOH were carried out because neutralization of the basic sites of guanidine by the free fatty acids present in the soybean oil can occur, deactivating the catalysts.[20]

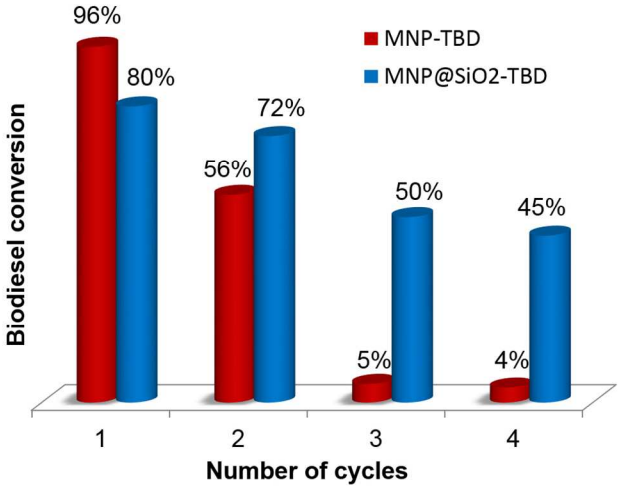


**Fig. 8** Reusability of the MNP-TBD and MNP@$SiO_2$-TBD nanocatalysts.

Fig. 8 shows the biodiesel yield upon four consecutive cycles using MNP-TBD and MNP@$SiO_2$-TBD. The activity of the MNP-TBD nanocatalyst was almost negligible after the fourth cycle. To understand why this deactivation occurred, elemental analysis of the MNP-TBD nanocatalyst was carried out after the fourth reaction cycle; the results indicated that only 0.03 mmol $g^{-1}$ of TBD remained on the magnetic support. Therefore, approximately 85% of the organic base was leached from the surface of the magnetic nanoparticles. Conversely, in the case of the MNP@$SiO_2$-TBD nanocatalyst, much better reusability was observed; elemental analysis of this nanocatalyst after the forth cycle revealed that approximately 23% of the TBD was leached (0.23 mmol $g^{-1}$ of TBD remained after the fourth cycle). Thus, the leaching process was more pronounced in the case of the magnetic nanocatalysts not coated with silica. To explain the difference in the leaching process between the two nanocatalysts, particle-size distribution (PSD) curves were obtained from TEM micrographs of MNP-TBD and MNP@$SiO_2$-TBD after the fourth cycle (Fig. 9).

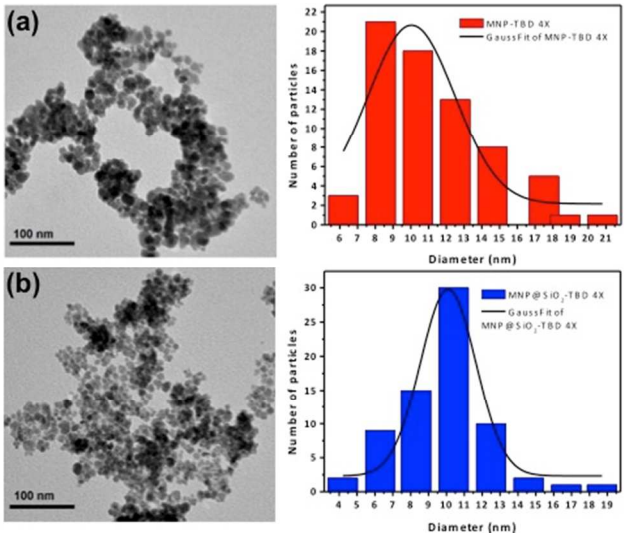


**Fig. 9** TEM microscopies and PSDs of (a) MNP-TBD and (b) MNP@$SiO_2$-TBD nanocatalysts after the forth cycle.

Fig. 9a shows that the PSD curve is shifted to smaller values compared to the PSD before the catalysis (Fig. 4a). In contrast, the PSD of MNP@$SiO_2$-TBD did not significantly change. These results indicate that the guanidine (TBD) leaching from the surface of MNP-TBD is associated with a partial dissolution of the iron oxide nanoparticles. Iron oxide nanoparticles can dissolve by different mechanisms in the presence of organic or inorganic acids.[44,45] At high temperatures (> 90 °C), the rate of iron oxide dissolution can increase. Because soybean oil is composed of a mixture of fatty acids, including linoleic and oleic acids,[46] the dissolution process can occur *via* the adsorption of these compounds onto the surface of the MNP-TBD nanocatalysts. Indeed Fig. 7 shows that the colour of the solution appears brown, indicating partial dissolution of iron oxide in the presence of fatty acids and also possible oxidation of $Fe_3O_4$ to $Fe_2O_3$. The silica coating protected the iron oxide nanoparticles from dissolution; consequently, MNP@$SiO_2$-TBD exhibited better reusability and structural stability than the MNP-TBD nanocatalyst under the conditions used in this work.

Several efforts have been carried out to obtain structurally stable catalysts in addition to good recyclability. Zhang *et al.*[47] prepared Pd/$Fe_3O_4$ binary superstructures for use in catalyzing dye degradation. Although the material exhibited good catalytic performance, the structural stability of the superstructures was quite poor. The low stability of the Pd/$Fe_3O_4$ binary superstructure was attributed to van der Waals week interactions between the particles that are short range in action. Coating the Pd/$Fe_3O_4$ binary particles with polypyrrole shell prevented the deconstruction of the superstructures and consequently, improved structural stability and reusability of the catalysts.[47] In the case of the MNP-TBD nanocatalyst investigated in this work, we believe that the poor stability of this material might be related to dissolution process due to the presence of fatty acids in the soybean oil. Thus, protecting iron oxide nanoparticles with polymers or oxides seems to be the best strategy to improve structural stability and recyclability of the magnetic catalysts.

## Conclusions

Three new recoverable magnetic nanocatalysts for biodiesel production were successfully prepared. All of the nanocatalysts exhibited superparamagnetic behaviour at room temperature and were observed to support methanolysis of soybean oil. The MNP-TBD nanocatalyst exhibited the best performance, with a biodiesel yield of 96% at 120 °C and 24 h of reaction time in the first cycle. The MNP-TMG nanocatalyst was the least efficient, most likely because of steric effects caused by its methyl groups. The nanocatalysts were easily recovered using an external magnetic field. The reusability of MNP@$SiO_2$-TBD was better than that of MNP-TBD because the silica coating protected the iron oxide nanoparticles from dissolution caused by the free fatty acids present in the soybean oil. The results of the present study demonstrated the advantages of using magnetic nanoparticles as catalytic supports instead of conventional supports; the magnetic supports are useful for the clean and economical production of biodiesel. These nanocatalysts can also be used for other reactions and might exhibit better reusability under neutral or basic reaction conditions.

## Experimental

### Materials and methods

The following reagents were used without any prior treatment: anhydrous iron(II) chloride, iron(III) chloride hexahydrate, CPTES 95%, tetraethyl orthosilicate (TEOS) 98%, 1,1,3,3-tetramethylguanidine (TMG), 1,5,7-triazabicyclo[4.4.0]dec-5-ene (TBD) from Sigma-Aldrich and ammonium hydroxide, triethylamine and ethanol from Vetec. Toluene (Vetec) was dried under sodium and subsequently distilled. Methanol (Vetec) and commercial soybean oil (LIZA) were used in the transesterification reaction without further purification. Fourier-transform infrared (FT-IR) spectra were recorded in the range from 400 to 4000 $cm^{-1}$ on a Varian 660-IR FT-IR spectrophotometer using the KBr pellet technique. The TGA of the samples was performed under flowing nitrogen (50 $cm^3$ $min^{-1}$) on a TG Instruments system, model Shimadzu DTG-60/60H; the samples were heated from 30 °C to 600 °C at a heating rate of 5 °C $min^{-1}$. Elemental analyses (CHN) were carried out using in a Perkin Elmer CHN 240 C analyser at the Central Analítica of the Instituto de Química, Universidade de São Paulo, Brazil. Powder XRD patterns were collected on a Bruker D8 Advance X-ray diffractometer equipped with a LynxEye detector and a Co-K$\alpha_1$ (1.78901 Å) and Co-K$\alpha_2$ (1.7929 Å) radiation source. The following databases were used: PDF 082-1533 for magnetite and PDF 039-1346 for maghemite, both from ICCD, 2003. Raman spectra were recorded with a Witec Alpha 300 confocal Raman imaging microscope. The experiments were performed at 25 °C using an Nd:YAG green laser with a wavelength of 532 nm and a small aperture (730 CCD cts for $SiO_2$) to avoid decomposition or phase changes in the sample during the analysis. The laser light was focused onto the sample using a 100× objective lens (NA = 0.95); the integration time was 0.5 s, and the number of scans was 600. Two different points were focused, allowing better characterization of the samples. TEM images were obtained using a JEOL JEM-1011. For these analyses, 1.0 mg of the samples was dispersed in 1 mL of ethanol by sonication for 10 min. A drop of this dispersion was transferred into 50 mL of deionized water, and a carbon-coated copper grid was subsequently immersed into this dispersion. This grid was stored in a desiccator for one week to slowly remove the solvent. The magnetic measurements were carried out in a magnetometer with a SQUID sensor (MPMS-XL, Quantum Design). The specific surface areas of the nanocatalysts were characterized by isotherms of $N_2$, which were obtained using an ASAP 2020 V304-4 serial 1200 apparatus. Prior to the measurements, the samples were degassed under vacuum at 100 °C for 24 h.

### Preparation of the magnetic nanoparticles (MNPs)

$Fe_3O_4$ nanoparticles were prepared by a chemical coprecipitation method.[32] $FeCl_3 \cdot 6H_2O$ (48.64 g, 180 mmol) and $FeCl_2$ (11.34 g, 89 mmol) were dissolved in 1 L of deionized water. The solution was degassed by bubbling Ar for 30 min at room temperature under mechanical stirring (400 rpm). Then, 100 mL of 25% $NH_4OH$ was quickly added in one portion to the solution. The reaction mixture remained under mechanical stirring and Ar atmosphere at RT for 1 h. The black precipitate was separated from the solution using magnetic decantation and was subsequently washed with deionized water (10×). The resulting black solid was dried under vacuum at RT for 5 h, yielding a compound labelled MNPs (21.00 g).

### Grafting of 3-(chloropropyl)triethoxysilane onto MNPs

MNPs (20 g) were dispersed in 400 mL of EtOH:$H_2O$ (1:1) by sonication for 1 h. The dispersion was then transferred to a round-bottom flask and heated to 40 °C under Ar atmosphere and mechanical stirring (300 rpm) for 30 min. After this period, 8 mL of CPTES (95%) was added. The reaction mixture remained under stirring for 3 h, after which five aliquots of 2 mL of CPTES were added during an interval of 6 h. The reaction mixture was left to stir for another 16 h, and the solid was collected by centrifugation (3000 rpm for 10 min) and washed with EtOH (3×). The final product was dried under vacuum at RT for 3 h and labelled as MNP-Cl.

### Preparation of guanidine-functionalized magnetic nanocatalysts

The MNP-Cl (8.0 g) was dispersed in dry toluene (50 mL) by being sonicated for 1 h and placed to a 250 mL round-bottom flask. The TBD (5.0 g, 36 mmol) in triethylamine (11 mL, 79 mmol) was added to the dispersion under mechanical stirring (300 rpm), and the reaction mixture was refluxed for 24 h. The final product was separated by magnetic decantation and washed sequentially (4×) with $CH_2Cl_2$, EtOH and $CH_2Cl_2$. The product was then dried under vacuum at RT for 2 h and labelled as MNP-TBD. The same procedure was followed for the synthesis of MNP-TMG except that, in this case, TMG (5 mL, 40 mmol) was used.

### Preparation of silica-coated MNPs

A one-step synthesis was used to obtain silica-coated $Fe_3O_4$ nanoparticles.[48] Tetraethylorthosilicate (TEOS) (2.7 mL) in EtOH (60 mL) was added to the reaction mixture of $Fe_3O_4$ nanoparticles. The reaction was continued for 24 h at RT. The resulting silica-coated MNPs were separated by magnetic decantation and alternately washed (9×) with $H_2O$ and EtOH. The

MNPs were then dried under vacuum at RT for 8 h, affording MNP@$SiO_2$.

**Grafting of 3-(chloropropyl)triethoxysilane onto silica-coated MNP**

MNP@$SiO_2$ (8.00 g) was dispersed in 200 mL of dry toluene by sonication for 1 h. The dispersion was subsequently refluxed under Ar atmosphere and mechanical stirring (800 rpm). After this period, 8 mL of CPTES was added and the reaction mixture remained under stirring for 6 h. Then, five 2 mL aliquots of CPTES were added during an interval of 3 h. The reaction mixture was left to stir for an additional 16 h. The solid was collected by magnetic decantation and washed with EtOH (6×). The final product was dried under vacuum at RT for 12 h, affording MNP@$SiO_2$-Cl.

**Guanidine functionalization of silica-coated magnetic nanocatalysts**

MNP@$SiO_2$-Cl (7.0 g) was dispersed in dry toluene (100 mL) by sonication for 1 h. Subsequently, TBD (4.0 g, 29 mmol) in triethylamine (5 mL, 36 mmol) was added to the dispersion under mechanical stirring (300 rpm) and the reaction mixture was refluxed for 24 h. The final product was separated by magnetic decantation, washed sequentially (7×) with $CH_2Cl_2$, EtOH and $CH_2Cl_2$, and dried under vacuum at RT for 8 h, affording MNP@$SiO_2$-TBD.

**Catalytic reactions**

The transesterification reactions were carried out in a Parr 5500 HP (100 mL) reactor under magnetic stirring and at a controlled temperature. The reactor was loaded with soybean oil and a methanolic suspension of the catalysts (10% w/w), which provided a 30:1 methanol-to-oil molar ratio. Prior to the reaction, the catalysts were dispersed in methanol by sonication for 1 h. The system was closed and heated to 120 °C for 24 h under an autogenous pressure. After this period, the reactor was cooled to RT and the catalysts were magnetically separated from the reaction mixture. The method used to analyse and quantify the biodiesel formed in the reaction is described elsewhere.[20] Briefly, we diluted (1% w/v) the lower phase (alkyl ester) in isopropyl alcohol and analysed it (in duplicate) using an Agilent 1200 high-performance liquid chromatograph. The products were separated using a 250 mm long column with 4.6 mm internal diameter; the column was packed with C18-covered silica with a particle size of 5 µm. A pre-column 2 cm in length was fitted between the injector and the separation column. The solvent gradient elution was performed using mobile phases A (methanol), B (*n*-hexane) and C (isopropanol). The phases were filtered through a membrane of expanded polytetrafluoroethylene (PTFE) with a diameter of 47 mm. Analyses were carried out at 40 °C and at a flow rate of 1 mL/min using spectrophotometric detection at 205 nm in the UV region. The sequence of the gradient was: at 0 min – 98% A, 1% B and 1% C; at 20 min – changed to 2% A, 49% B and 49% C; at 22 min – 98% A, 1% B and 1% C. The peaks were identified by comparison of the retention times of the samples with those of standard compounds (triglyceride and fatty acid methyl esters). The chromatograms, which were analysed and integrated with the aid of the Agilent ChemStation software, were used to quantify the amount of methyl fatty esters (biodiesel) formed in the reactions on the basis of the response factor obtained from a previously constructed calibration curve.

**Reusability of the catalysts**

The catalysts used in the first cycle of the transesterification reactions were separated from the reaction solution using a magnet, recovered, extensively washed with methanol, and then washed with 0.1 mol $L^{-1}$ NaOH aqueous solution and deionized water until the pH of the suspension was 7. The catalysts were air-dried before reuse in the next cycle. Each catalyst was then used in a new reaction cycle under the previously described conditions.

## Acknowledgements

The authors gratefully acknowledge FAPERJ (JCNE), CNPq (Jovens Pesquisadores em Nanotecnologia grant number 550572/2012-0 and ECSS fellowship) and CAPES (T.C.S. fellowship) for financial support. C.M.R. is recipient of a CNPq research fellowship. We thank Prof. Cláudio J. A. Mota and Ana L. Lima (IQ-UFRJ, Brazil) for assistance with the catalytic experiments. We also thank the Multiuser Laboratory of Material Characterization (http://www.uff.br/lamate/) and Multiuser Laboratory of Microscopy (Rômulo Custódio dos Santos).

## Notes and references

[a] *Instituto de Química, Universidade Federal Fluminense, Campus do Valonguinho, CEP 24020-141, Niterói, Rio de Janeiro, Brazil; E-mail: cmronconi@id.uff.br*
[b] *Instituto de Física, Universidade Federal Fluminense, Campus da Praia Vermelha, Niterói-RJ, Brazil.*
[c] *Instituto de Física, Universidade de São Paulo, CP 66318, 05314-970 São Paulo, SP, Brazil.*
*†Electronic Supplementary Information (ESI) available. See DOI: 10.1039/b000000x/*

1 N. F. Nasir, W. R. W. Daud, S. K. Kamarudin and Z. Yaakob, *Renew. Sust. Energ. Rev.*, 2013, **22**, 631.
2 G. Knothe, J. Gerpen and J. Krahl. The biodiesel handbook. Urbana, Illinois: AOCS Press, 2005.
3 A. Islam, Y. H. Taufiq-Yap, C.-M. Chu, E.-S. Chan and P. Ravindra, *Process. Saf. Environ.*, 2013, **91**, 131.
4 K. Ramachandran, T. Suganya, N. N. Gandhi and S. Renganathan, *Renew. Sust. Energ. Rev.*, 2013, **22**, 410.
5 U. Schuchardt, R. Sercheli and R. M. Vargas, *J. Braz. Chem. Soc.*, 1998, **9**, 199.
6 I. M. Atadashi, M. K. Aroua, A. R. A. Aziz and N. Sulaiman, *J. Ind. Eng. Chem.*, 2013, **19**, 14.
7 D.-W. Lee, Y.-M. Park and K.-Y. Lee, *Catal Surv. Asia*, 2009, **13**, 63.
8 E. Santacesaria, G. M. Vicente, M. Di Serio and R. Tesser, *Catal. Today*, 2012, **195**, 2.
9 K. G. Georgogianni, A. P. Katsoulidis, P. J. Pomonis and M. G. Kontominas, *Fuel Process. Technol.*, 2009, **90**, 671.
10 J. Shen, J. Kobe, Y. Chen and J. Dumesic, *Langmuir*, 1994, **10**, 3902.
11 G. J. Suppes, M. A. Dasari, E. J. Doskocil, P. J. Mankidy and M. J. Goff, *Appl. Catal. A- Gen.*, 2004, **257**, 213.
12 S. K. Karmee and A. Chadha, *Bioresource Technol.*, 2005, **96**, 1425.
13 M. Di Serio, R. Tesser, L. Pengmei and E. Santacesaria, *Energ. Fuels*, 2008, **22**, 207.
14 Y. B. Cho and G. Seo, *Bioresource Technol.*, 2010, **101**, 8515.
15 M. R. Mello, D. Phanon, G. Q. Silveira, P. L. Llewellyn and C. M. Ronconi, *Microporous Mesoporous Mater.*, 2011, **143**, 174.

16 T. C. Santos, S. Bourrelly, P. L. Llewellyn, J. W. de M. Carneiro and C. M. Ronconi, *Phys. Chem. Chem. Phys.*, 2015, **17**, 11095.
17 G. Q. Silveira, M. D. Vargas and C. M. Ronconi, *J. Mater. Chem.*, 2011, **21**, 6034.
18 G. Q. Silveira, R. S. da Silva, L. P. Franco, M. D. Vargas and C. M. Ronconi, *Microporous Mesoporous Mater.*, 2015, **206**, 226.
19 J. M. Balbino, E. W. Menezes, E. V. Benvenutti, R. Cataluña, G. Ebeling and J. Dupont, *Green Chem*., 2011, **13**, 3111.
20 A. L. Lima, A. Mbengue, R. San Gil , C. M. Ronconi, C. J. A. Mota, *Catal. Today*, 2014, **226**, 210.
21 D. Meloni, R. Monaci, Z. Zedde, M. G. Cutrufello, S. Fiorilli and I. Ferino, *Appl. Catal. B- Environ*., 2011, **102**, 505.
22 R. Sercheli, R. Vargas and U. Schuchardt, *J. Am. Oil Chem. Soc.*,1999, **76**, 1207.
23 S. Paria and R. Chaudhuri, *Chem. Rev*., 2012, **112**, 2373.
24 H.-J. Xu, X. Wan, Y. Geng and X.-L. Xu, *Curr. Org. Chem*., 2013, **17**, 1034.
25 L. M. Rossi, N. J. S. Costa, F. P. Silva and R. Wojcieszak, *Green Chem*., 2014, **16**, 2906.
26 Zillillah, T. A. Ngu and Z. Li, *Green Chem.*, 2014, **16**, 1202.
27 Z. Chen, W. Xu, L. Jin, J. Zha, T. Tao, Y. Lin and Z. Wang, *J. Mater. Chem A*, 2014, **2**, 18339.
28 Zillillah, G. Tan and Z. Li, *Green Chem*., 2012, **14**, 3077.
29 C. G. S. Souza, W. Beck and L. C. Varanda, *J. Nanopart. Res.*, 2013, **15**, 1545.
30 A. Rostami, B. Atashkar and D. Moradia, *Appl. Catal. A- Gen*., 2013, **467**, 7.
31 M. Ma, Y. Zhang, W. Yu, H.-Y. Shen, H.-Q. Zhang and N. Gu, *Colloid Surface A*, 2003, **212**, 219.
32 B. Atashkar, A. Rostami and B. Tahmasbi, *Catal. Sci. Technol*, 2013, **3**, 2140.
33 F. Galeotti, F. Bertini, G. Scavia and A. Bolognesi, *J. Colloid Interf. Sci*., 2011, **360**, 540.
34 R. A. Bini, R. F. C. Marques, F. J. Santos, J. A. Chaker and M. Jafelicci Jr., *J. Magn. Magn. Mater.*, 2012, **324**, 534.
35 F. Adam and M. S. Batagarawa, *Appl. Catal. A- Gen.*, 2013, **454**, 164.
36 A. C. Blanc, D. J. Macquarrie, S. Valle, G. Renard, C. R. Quinn and D. Brunel, *Green Chem*., 2000, **2**, 283.
37 L. Signorini, L. Pasquini, L. Savini, R. Carboni, F. Boscherini, E. Bonetti, A. Giglia, M. Pedio, N. Mahne and S. Nannarone, *Phys. Rev. B*, 2003, **68**, 195423.
38 N. Pinna, S. Grancharov, P. Beato, P. Bonville, M. Antonietti and M. Niederberger, *Chem. Mater.*, 2005, **17**, 3044.
39 C. S. S. Kumar (Ed.): Raman Spectroscopy for Nanomaterials Characterization. London: Springer-Verlag Berlin Heidelberg, 2012.
40 M. C. Mascolo, Y. Pei and T. A. Ring, *Materials*, 2013, **6**, 5549.
41 F. Márquez, T. Campo, M. Cotto, R. Polanco, R. Roque, P. Fierro, J. M. Sanz, E. Elizalde and C. Morant, *Soft Nanosci. Lett.*, 2011, **1**, 25.
42 U. Gradmann, *J. Magn. Magn. Mater.*, 1991, **100**, 481.
43 T. Ishikawa (ed.). Superbases for organic synthesis: guanidines, amidines and phosphazenes and related organocatalysts. West Sussex: John Wiley & Sons Ltd, 2009.
44 D. Panias, M. Taxiarchou, I. Paspaliaris and A. Kontopoulos, *Hydrometallurgy*, 1996, **42**, 257.
45 B. Kalska-Szostkoa, U. Wykowska, K. Piekut, D. Satuła, *Colloid Surfaces A*, 2014, **450**, 15.
46 S. P. Singh and D. Singh, *Renew. Sust. Energ. Rev.*, 2010, **14**, 200.
47 X. Zhang, M. Lin, X. Lin, C. Zhang, H. Wei, H. Zhang and B. Yang, *ACS Appl. Mater. Interfaces*, **2014**, *6*, 450.
48 N. Chekiva, D. Horák, P. Jendelová, M. Trchová, M. Benes, M. Hrubý, V. Herynek, K. Turnovcová and E. Syková, *J. Mater. Chem*., 2011, **21**, 7630.